SAND2017-9645R

Built on
LDRD
Laboratory Directed Research
and Development

SAND20XX-XXXXR
LDRD PROJECT NUMBER: 181205
LDRD PROJECT TITLE: Lithium Oxysilicate Compounds
PROJECT TEAM MEMBERS: Chris Apblett, Jaclyn Coyle

ABSTRACT:

In this study, the structure and composition of lithium silicate thin films deposited by RF magnetron co-sputtering is investigated. Five compositions ranging from $Li_2Si_2O_5$ to Li_8SiO_6 were confirmed by inductively coupled plasma-optical emission spectroscopy (ICP-OES) and structure analysis on the evolution of non-bridging oxygens in the thin films was conducted with fourier transform infrared (FTIR) spectroscopy. It was found that non-bridging oxygens (NBOs) increased as the silicate network breaks apart with increasing lithium content which agrees with previous studies on lithium silicates. Thin film impurities were examined with x-ray photoelectron spectroscopy (XPS) and time of flight secondary ion mass spectroscopy (TOF-SIMS) and traced back to target synthesis. This study utilizes a unique synthesis technique for lithium silicate thin films and can be referred to in future studies on the ionic conductivity of lithium silicates formed on the surface of silicon anodes in lithium ion batteries.

INTRODUCTION:

Lithium ion batteries are currently the power source of choice for portable electronics and hybrid electric vehicle applications due to their outstandingly high energy density [1, 2]. Typical commercial lithium batteries are made with graphite anodes with a specific capacity of about 372 mAh/g[3]. Silicon anodes have a theoretical capacity of about 3600 mAh/g, low overpotential, fast reaction kinetics and is the second most abundant element on earth[3, 4]. In principle, this puts silicon at the top of the list of material that could replace the graphite anodes and help make lithium ion batteries more suitable for electric vehicle applications[5]. However, silicon has an unstable solid electrolyte interface (SEI) layer that, among other components, includes lithium silicates. These lithium silicates and the unstable SEI layer lead to silicon having initial irreversible capacity losses, poor cycling stability and a limited cycle life[6-8]. While both organic containing species as well as lithium silicates have been identified as constituents within the SEI, the nature and effect of the inorganic phases within the silicon SEI have not been well characterized.

In order to fully understand the effect of these lithium silicates on silicon anodes and cell cycling, the lithium silicates themselves need to be studied. Once the lithium silicates are more fully understood on their own, they can be used as model SEI layers to study lithiation of the native oxide on a silicon anode. There are many studies on lithium silicates using bulk synthesis techniques such as solid state reactions/glass melts or sol gel to form powders[9-15] as well as thin film techniques like pulsed laser deposition, RF magnetron sputtering and sol gel spin coating[16-18], but these studies have a limited range of compositions assessed, and don't necessarily match the compositions of lithium silicates found within the SEI layers. In addition, there has been some evidence of time evolution of the silicates upon cell cycling in silicon based on electrolyte additives[8], which further confounds the understanding of the role of the lithium silicates formed from the lithiation of native oxide on silicon anode cell performance. In studies examining the composition of the SEI components formed on silicon, the most common lithium silicate observed is lithium orthosilicate (Li_4SiO_4)[6, 19-21] with a few studies also mentioning lithium metasilicate (Li_2SiO_3)[22] or lithium disilicate ($Li_2Si_2O_5$)[20]. A few studies have explored higher lithium content lithium silicate powders such as lithium orthosilicate or oxolithium silicate (Li_8SiO_6)[10], but most have been done on lithium disilicate or lithium metasilicate[13, 14, 23, 24].

Since the native oxide layer on silicon has been observed to be between 2-10 nm [20, 25, 26] and the typical SEI layer formed on the silicon surface is also in the range of 25-300nm [22, 27], it is evident that any model layer used to study these layers must also be a thin film. To create lithium silicate thin films that could be used as such a model layer, we have chosen to use an RF Magnetron co-sputtering technique. The only previous study using sputtering to deposit lithium silicate films sputtered off of stoichiometric Li_2SiO_3 and Li_4SiO_4 targets and showed that films deposited from this single target method were lithium deficient due to lithium segregation in the sputter targets with continued sputtering [18]. Co-sputtering off of an Li_2O and an SiO_2 target provides more freedom in the range of compositions produced and prevents discrepancies in composition between stoichiometric single targets and the thin films deposited.

An in depth analysis of the structure of sputtered amorphous thin film lithium silicates ranging in composition from $Li_2Si_2O_5$ (1:1 Li/Si) to Li_8SiO_6 (8:1 Li/Si) has not been done experimentally before. The structure is important because it is related to the ionic conductivity of the lithium silicates is critical for silicon anode applications. Studies that have looked at a range of structures are mostly theoretical studies using molecular dynamic calculations [28-31]. In particular, a study by Kim et al. predicted the composition evolution of lithium silicates sequentially from $Li_2Si_2O_5$ to Li_4SiO_4 as the SiO_2 layer of a silicon anode [28]. There have been no studies verifying the formation of each of these lithium silicate compositions specifically or on how they affect silicon anode performance. In this study, to further the understanding of the formation of the SEI on a silicon anode, compositions ranging from $Li_2Si_2O_5$ to Li_8SiO_6 of model SEI lithium silicate thin films were synthesized through RF magnetron co-sputtering and structural analysis was completed to be applied in further studies using these model SEI layers.

DETAILED DESCRIPTION OF EXPERIMENT/METHOD:

Amorphous lithium silicate films about 550 nm thick were deposited on 1cmx1cm substrates of either silicon, potassium chloride or platinum coated stainless steel by means of radio-frequency magnetron co-sputtering of a SiO_2 (99.995%, Kurt J. Lesker) target and a homemade Li_2O target in a pure Argon (99.999%, Airgas) atmosphere. All depositions were made with a Kurt J. Lesker PVD 75 system. The Li_2O target was made from pressed disks of lithium dioxide powder (97% 9060 mesh, Aldrich). These disks were calcined at 900C for 10 hours separated by carbon paper to prevent disks from fusing together. The SiO_2 target was sputtered under a range of powers from 9 – 28W while the Li_2O target was sputtered under a constant power of 20W for all compositions to achieve different Li/Si ratios. Both targets were sputtered into a target blank for at least 40 minutes before actual deposition to avoid cross-contamination. During deposition, the substrate holder was rotated in order to achieve homogeneous films. Film deposition rates varied between 3 to 7.5 angstroms/minute. Deposition times were controlled to achieve the desired thickness for each film. Film thickness measurements were made with a Dektak 3030 profilometer. Each sample was replicated at least XXX times for reproducibility and error analysis.

Composition analysis was done using a ARL 3410+ inductively coupled optical emission spectrometer (ICP-OES). Samples were deposited onto potassium chloride crystals (Sigma Aldrich) and dissolved in water prior to being fed to the plasma. Structural analysis of the films was carried out by using a Nicolet Instruments Nexus 670 fourier transform infrared spectrometer (FTIR). Measurements were taken under a nitrogen atmosphere in transmission mode in the range 4000-400 cm^{-1} with 809 scans for each sample. Film surface and depth profiling was completed with a Kratos Axis Ultra DLD x-ray photoelectron spectrometer (XPS) with a base pressure of less than $5x10^{-9}$ Torr. 120 W monochromatic Al Kα (1486.7 eV) x-rays were utilized for excitation. Samples were transferred straight from an Argon filled glovebox to the XPS spectrometer using an air-tight transfer rod. A Kratos Minibeam III ion gun operating at 4kV Ar^+ with 1 microamp current over a 4x4 mm square area was used during sputtering for depth analysis. The binding energy spectra were calibrated during data processing by adjusting the C 1s (C-C) peak to 284.8 eV using CasaXPS Version 2.3.15. Similar analysis was completed with an Ion-TOF time of flight secondary ion mass spectrometer (TOF-SIMS). Samples were transferred from an argon filled glovebox using an inert atmosphere sample transfer pod to avoid exposure to air. A 25 keV Bi^{1+} beam with a $100x100μm^2$ raster was utilized to analyze negative secondary ions. For depth profiling a 1keV Cs+ sputtering beam was used over a $300x300μm^2$ area. A low energy (20eV) electron flood gun was used for charge compensation initially until it was found that the films changed in appearance when exposed to low energy electrons. All data are presented as normalized to ^{30}Si.

RESULTS:

Composition, morphology and thickness of thin films

The ICP-OES results of the thin film sputtered onto KCl substrates are shown in Figure 1. According to the results of the elemental analysis, there is a linear relationship between the ratio of powers on the Li_2O and SiO_2 target and the lithium to silicon ratio in the thin films. There is only a small error associated with each power setting intended for the following compositions: Li/Si = 1.4, 1.9. 2.9, 4.8 and 7.7. The error bars are an indication of consistency for multiple depositions. The data in this graph represents 7 different deposition runs for each composition. Film deposition rates varied between 3 to 7.5 angstroms/minute. Deposition times were controlled to achieve the desired thickness for each film (~550nm). The time for each deposition ranged from 14 hours to 26 hours with runs using lower Li_2O/SiO_2 target ratios requiring longer deposition times to achieve the 550nm thickness goal.

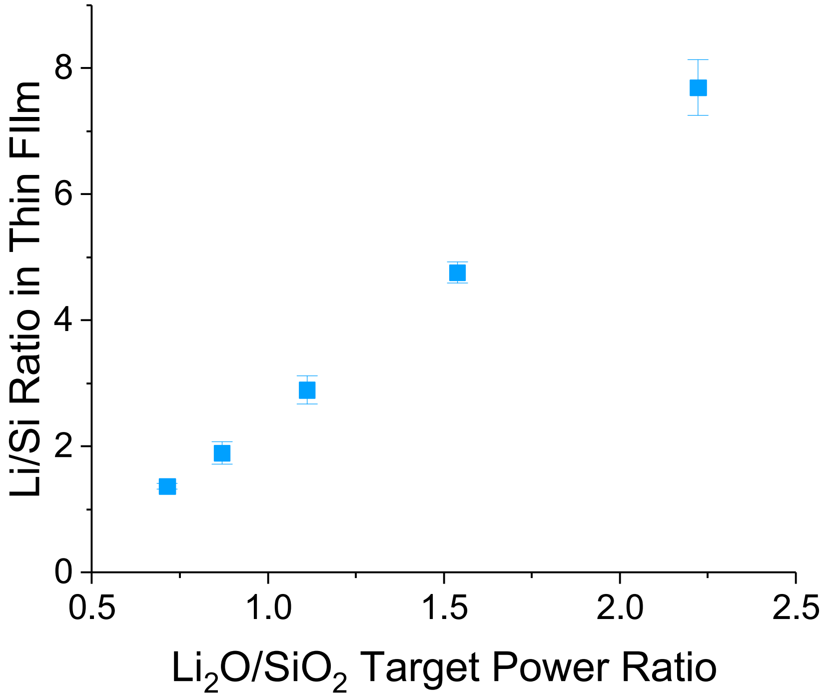

Figure 1: ICPOES results for Li/Si ratio in each thin film at each power setting

Structure/Composition in the bulk and with depth

Fourier Transform Infrared (FTIR) in transmission mode was used to examine the bulk structure of the sputtered lithium silicate samples. Figure 2 shows the full FTIR spectra of all 5 composition of sputtered lithium silicates. The peaks ~1450 cm^{-1} and ~880 cm^{-1} are consistent for all five compositions and are characteristic of Li_2CO_3 [32]. The small, but visible, peak at ~3700 cm^{-1} is from O-H stretching vibrations and is characteristic of LiOH[33]. Since these spectra are from bulk transmission mode IR spectroscopy, there is no information on whether the Li_2CO_3 and LiOH species are in the bulk of the film or are from surface contamination during transfer to the FTIR spectrometer. This will be discussed further with the surface analysis results.

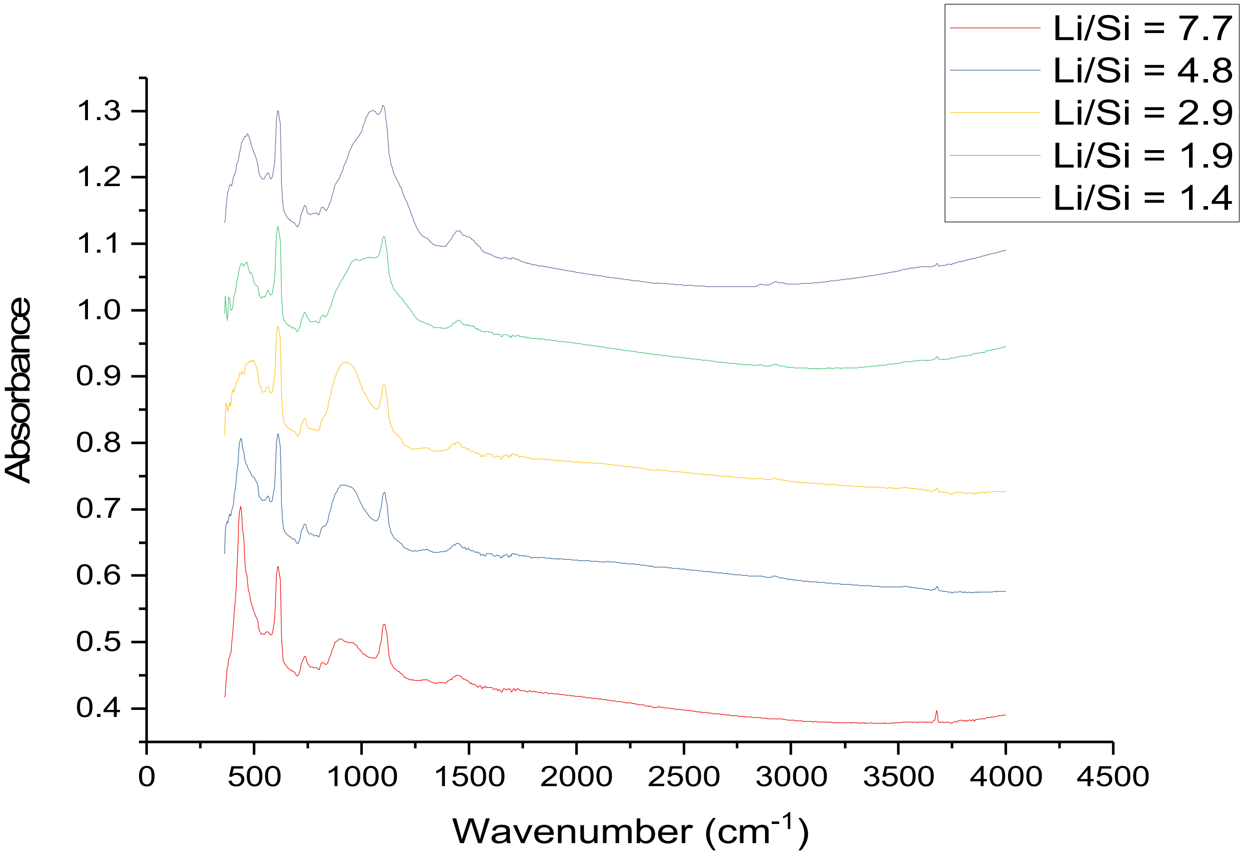

Figure 2: FTIR spectrum of all 5 sputtered lithium silicate compositions

The absorption peaks in the range 400 – 1200 cm^{-1} for FTIR are characteristic of silicate vibration modes as well as Li-O bonds so they can be used to compare the ratio of Li-O style bonds to bridging silicate network vibrations to characterize how disrupted the silicate network is for each lithium silicate composition we sputtered. The bond vibrations modes associated with each absorption peak in this region based on the literature are summarized in Table 1[13, 34-36]. The symmetric or asymmetric stretching vibration bands (ν_s or ν_{as}) at around 1160, 1100, 1000, 900 and 740 cm^{-1} were attributed to ν_{as}(Si-O-Si), ν'_{as}(Si-O-Si), ν_s(O-Si-O), ν(Si-O-) and ν_{as}(Si-O-Si) respectively. The lower wavenumber bands at around 600 corresponded to ν_s(Si-O-Si) and the wavenumbers around 500 to 560 cm^{-1} corresponded to the deformation vibrations δ(O-Si-O) or δ(S-O-Si). The bands centered around 440 cm^{-1} were due to deformation vibrations of the non-briding oxygen Si-O-(Li$^+$) type bonds and Li-O symmetric stretching vibrations of Li-O bonds in the Si?O_4 tetrahedra. Due to the constraints of the FTIR instrument we used, we could not see the asymmetric stretching vibrations of these Li-O bonds under 400 cm^{-1} that are known to occur in higher order lithium silicates[10, 37]. The location of each vibration mode shifts to slightly lower frequencies as the lithium content in each lithium silicate compostion increases. This makes sense because for FTIR, lower frequencies correspond to lower bond strength and as more weak Li bonds are added to the structure of the silicates, the entire network of the bulk structure grows weaker.

Table 1: Vibration mode assignments for FTIR peaks

Wavenumber (cm^{-1})	Vibration Mode Assignment
~440	δ(Si-O-(Li+)) and ν(Li-O)
~500, ~560	δ(O-Si-O) δ(S-O-Si)
~600	ν_s(Si-O-Si)
~740	ν_{as}(Si-O-Si)
~900	ν(Si-O-)
~1000	ν_s(O-Si-O)
~1100	ν'_{as}(Si-O-Si)
~1160	ν_{as}(Si-O-Si)

DISCUSSION:

The Gaussian peak deconvolution of this lithium silicate characteristic region for the thin film with a Li/Si = 7.7 composition ratio is shown in Figure 3 as an example to the method. The Gaussian peak fits were also completed for the other four compositions as well, with similar results. The peak positons remained the same as those described in Table 1 for all 5 compositions, but the intensity of the peaks shifted in a way that was indicative of increasing non-bridging oxygens (NBOs) as more lithium was added to the silicate network for higher lithium content lithium silicate films. A quantitative look at how these peaks shifted is shown in Figure 4 by comparing the peak integration for the most relevant vibration modes to the thin film structure as the lithium content increases. The peaks that do not change much across compositions (~600, 740 and 1100 cm^{-1}) are also too sharp to be associated with an amorphous material. Since sharp peaks in FTIR are indicative of a more ordered structure, these band have been assumed to come from the crystalline silicon substrate. The crystalline substrate shows up in the FTIR spectra because the spectrometer was in transmission mode. The vibration modes that are most sensitive to the structure of the lithium silicate films are ν(Si-O-) at ~900 cm^{-1} and δ(Si-O-(Li+)) and ν(Li-O) at ~440 cm^{-1} for the relative amount of NBOs in the material versus ν_s(O-Si-O) at ~1000 for the relative amount of BOs in the material. The fraction of ν_s(O-Si-O) at ~1000 cm^{-1} in Figure 4 (green) indicates that the number of BOs in the thin film decreases steadily as more lithium is added to the material and breaks apart the silicate network. Up to Li/Si = 3, as lithium is added to the silicate network and the silicate chains break apart, more NBO bonds are observed and increased Li-O vibrations are observed as well. As more lithium is added past Li/Si = 3, enough lithium is added that it is possible thatO^{2-} species begin to form, creating a decrease in NBOs as they dissociate with Si^{4+} altogether. This process can be observed by watching how the ν(Si-O-) density at 900 cm^{-1} (shown in purple) increases up to Li/Si = 3 and then decreases again for higher lithium content films. In conjunction with that trend, the δ(Si-O-(Li+)) and ν(Li-O) at ~440 cm^{-1} (shown in blue) increases as the lithium content increases as well, suggesting that more lithium is bonding into the silicate network. The δ(Si-O-(Li+)) and ν(Li-O) at ~440 cm^{-1} vibration bonds do not increase as much as would be expected compared to the decrease in ν(Si-O-) at 900 cm^{-1} , possibly because there is missing information about the Li-O bonds at frequencies < 400 cm^{-1}.

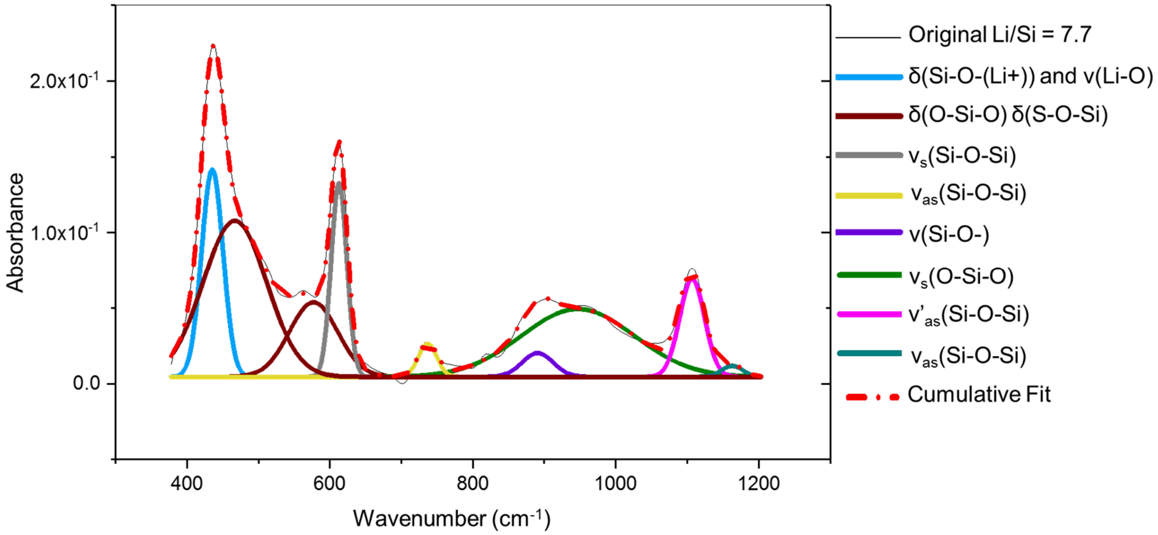

Figure 3: Gaussian peak deconvolution of Li/Si =9 film

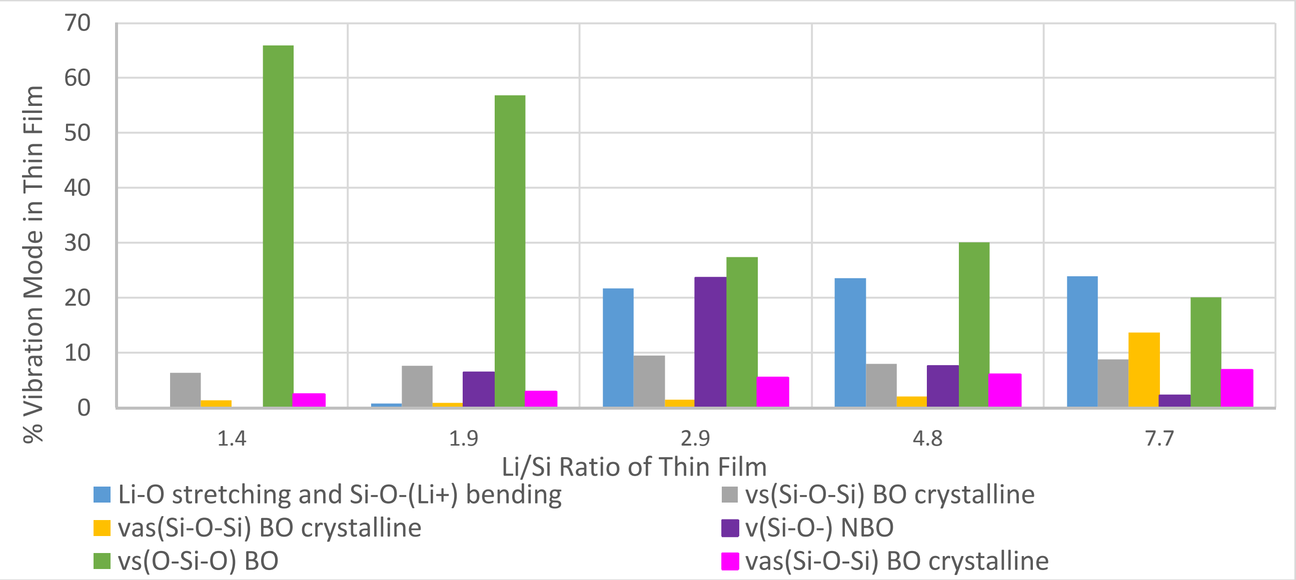

Figure 4: Percent of vibration modes relevant to lithium silicate film with for each composition

We now have an in-depth understanding of how increasing lithium content breaks apart the silica network. This bulk structure analysis is an important building block for understanding how lithium moves through the lithium silicate thin films. To our knowledge, this the the first instance of detailed structure analysis of lithium silicates with this range of compositions.

The next step in understanding these model lithium silicate layers for use on silicon anodes would be to understand the amount of lithium sites available vs concentration of lithium in the material effect Li mobility. Prior to this study, we performed surface analysis to make sure the carbonate/Li_2CO_3 vibration modes seen in FTIR were just from negligible surface contamination and not from bulk contamination of the material. Further bond analysis from XPS and TOF-SIMS should address the relative contribution of surface carbon vs. bulk carbon in the samples.

XPS was taken on all five compositions with depth profiling using an argon ion beam to avoid chemical interaction with the ion beam and the sample surface. Since lithium silicates are an oxide which typically have insulating properties, a low energy electron flood gun was used to compensate for the positive charge that builds up on insulating samples without it. Each sample was sputtered down past the top contamination layer (~ 210 seconds) in order to examine the bulk binding of the material. Figure 5 shows the O 1s, Si 2p, C 1s and Li 1s spectra of the Li/Si = 1.4 lithium silicate as well as a table of peak assignments from literature[6-8]. Each of these spectra can be split up into two

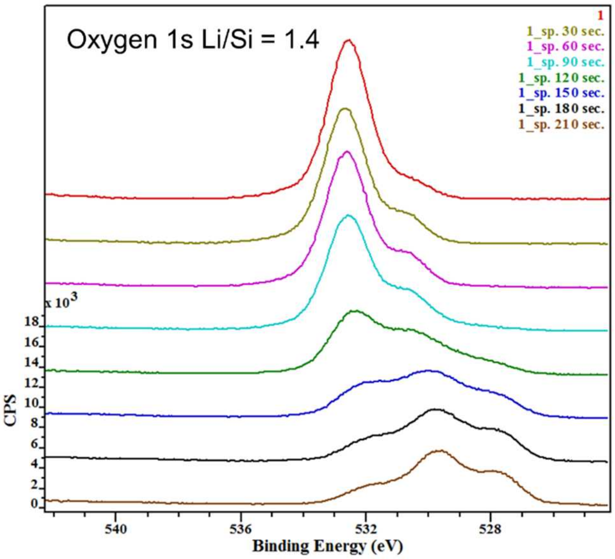

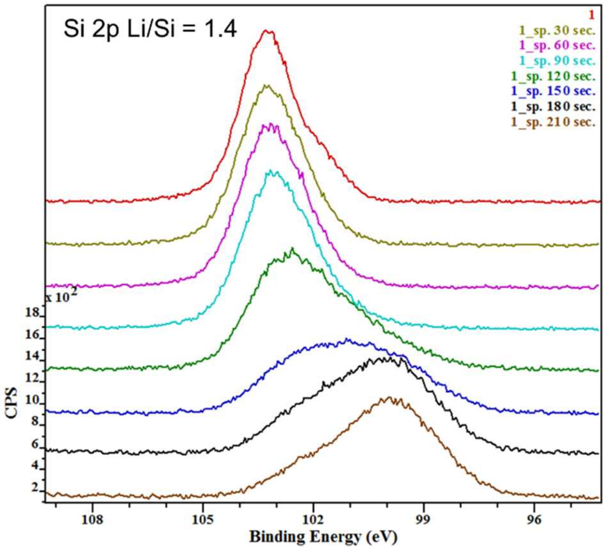

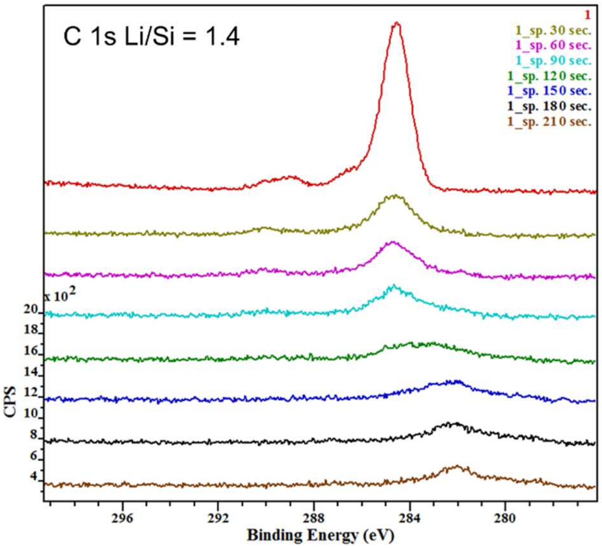

Binding Energy Region	Peak (eV)	Assignment
O 1s	532.7	SiO_2
	531	LiOH
	531.5	Li_2CO_3
	530-530.5	Li_xSiO_y
	528-528.5	Li_2O
C 1s	290	Li_2CO_3
	288.5	CO_2
	286.5	C-O
	284.6	C-C
Si 2p	103.2	SiO_2
	100.5 – 101.3	Li_xSiO_y

Figure 5: XPS depth profiling of O1s, Si 2p, C 1s and Li1s peaks in Li/Si = 1.4 sample and table of peak assignments

layers: the surface contamination layer on top of the film and the bulk film binding energies that show up after the rough transition zone at 120s of sputtering (green line). From the peaks at around 532.7, 531.5 and 531 eV on the O 1s spectra, the top contamination surface of the lithium silicate consists of SiO_2, Li_2CO_3, and LiOH respectively. The peak at around 290 eV for the C1s spectra and the peak at around 103.2 eV for the Si 2p spectra also support the presence of Li_2CO_3 and SiO_2 at the surface of the thin film. Once past the interface of the oxide layer and the bulk thin film structure, some charging issues begin to appear. This is most likely caused by differential charging which occurs in layered systems where the conductivity varies with each layer[38, 39]. As a results of this charging effect, the peaks in the bulk of the thin film appear to shift to lower binding energies by the action of the charge neutralizer, or electron flood gun, and are broadened slightly. This makes assigning these peaks to specific bonding structures challenging. For the purpose of our analysis, we have chosen to assign peaks based on a uniform shift to lower binding energies that correlates to the binding energies from known materials on the surface. There are three main peaks that show up between 528 and 532 eV in the bulk of the thin film for the O 1s spectra. Taking into account a slight shift to lower eV as mentioned, we have assign the peaks to SiO_2 (532.7 eV), Li_xSiO_y (530-530.5 eV) and Li_2O (528-528.5 eV). The presence of a SiO_2 as well as a Li_xSiO_y can be explained as the Li/Si = 1.4 thin film has the lowest amount of lithium in the silicate network. This indicates that there may be some nano-scale phase separation in these films. The Li_2O is mostly likely also a product of the charging effects in this material, as a reductive product of lithium ions, electrons from the flood gun and O_2 ions in the material (see equation 1)[40].

$$4Li^{+} + 4e^{-} + O_2 \rightarrow 2Li_2O \qquad E^o = 2.91\ \text{V} \tag{1}$$

The bulk bonding energies in the bulk of the thin film in the Si 2p spectra show a decrease in the SiO_2 peak at 103.2 and a shift toward Li_xSiO_y at 100.5 – 101.3 eV. Looking at the surface with the C 1s spectra, there appears to be extensive carbon contamination past just Li_2CO_3. There are peaks at 288.5 eV, 286.5 eV and 284.6 eV assigned to CO_2, C-O type bonds and C-C bonds. The Li_2CO_3, CO_2, and C-O bonds are expected from general surface reactivity with from any accidental exposure to the atmosphere, but the C-C bonds are unusual. The fact that these C-C continue on into the bulk of the lithium silicate thin film material (taking into account charge effects again), is indicative of a bulk contamination of higher order carbon, such as graphite, in the thin film.

This high order carbon contamination was verified with TOF-SIMs. Figure 6 shows that high order carbon species even up to C_4 are present in the bulk of the lithium silicate film Li/Si = 1.4. These highly ordered carbon species were seen in all 5 compositions of the lithium silicates we sputtered. It is highly unlikely such highly ordered carbon would come from air contamination or handling of samples. We believe this contamination came from the sintering step of the synthesis process of the target used for sputtering. The Li_2O target disks were separated by graphite sheets in the furnace to keep them from melding together. The graphite sheets visibly transferred some carbon onto the surface of the targets. The targets were mechanically abraded to attempt to get the graphite off and sputtered off of for 24 hours before deposition process began, but there is still evidence of contamination in the films. However, even though this carbon exists within the films, there is no reason that it should affect the analysis on the silicate and lithiate structures, which lend further evidence to the disruption of the silicate network as the lithium content is increased.

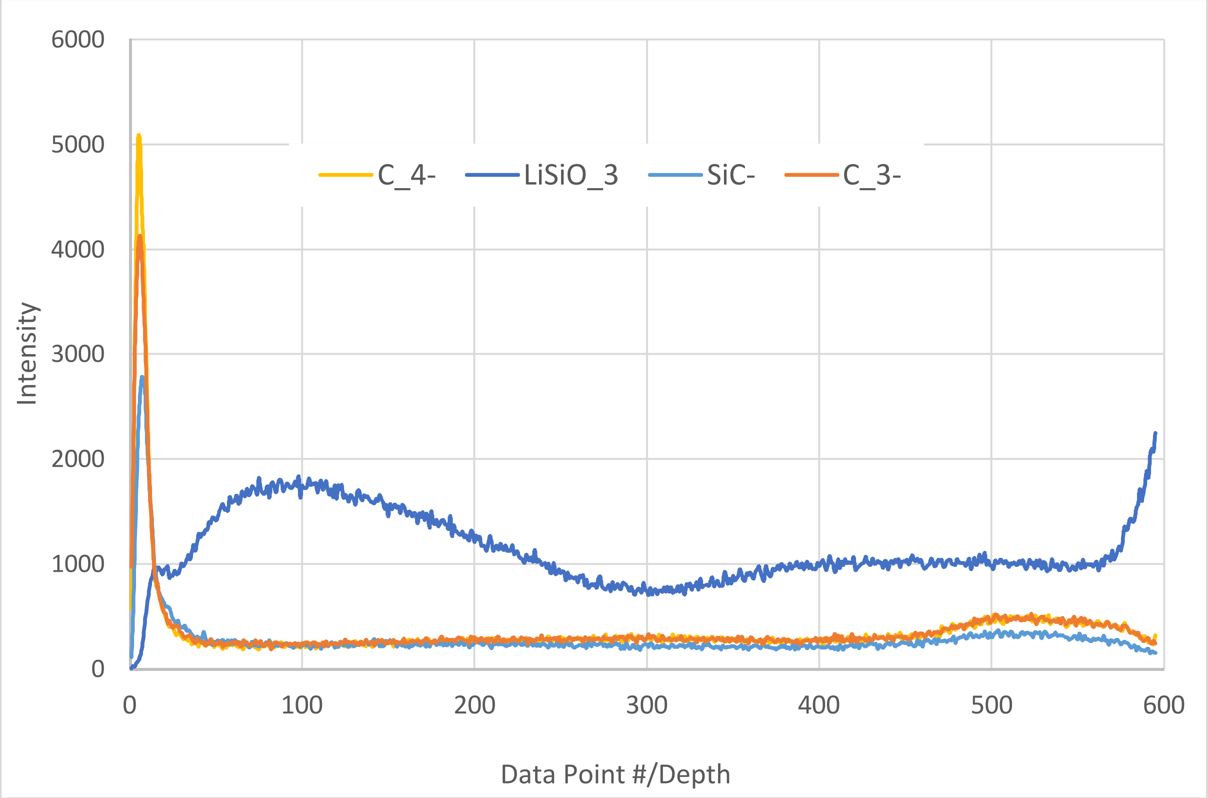

Figure 6: TOF-SIMS analysis of Li/Si = 1.4 thin film

ANTICIPATED OUTCOMES AND IMPACTS:

The campus executive program supported one full time student from the University of Colorado, Boulder, for this activity. The student has been part of the activity from the beginning, and helped to define the work that is presented here. The work resulted in one paper in submission to the Journal of Vacuum Science and Technology, and also two Electrochemical Society presentations given by the student. Another journal article is currently in manuscript preparation, and another conference presentation will happen in the fall of 2018.

The other major outcome from this work was the development of a successfully funded proposal surrounding the idea of Silicon anode electrode fundamental studies. Lead by the National Renewable Energy Laboratory, this proposal focused on understanding the basic issues surrounding the function of Si as an anode material, and why the capacity, coulombic efficiency, and cycle retention for these materials was so poor. Initially over 10x the capacity of state of the art current anodes, these materials quickly lose capacity and become nonfunctional after a few dozen charge/discharge cycles. The study of lithium oxysilicates as a barrier or engineered interfacial layer between the electrolyte and the silicon anode helped to convince the funding agencies that Sandia could contribute a good scientific basis by carefully controlling the chemistry of these interfaces, and observing as the interfaces evolved over time. By understanding how the starting chemistry affected these developments, key insights into the mechanisms for degradation can be elucidated.

CONCLUSION:

A well characterized model SEI is necessary to observe intricate changes caused by cycling of the silicon anode. The results of our study allowed us to evaluate whether this synthesis technique gave us adequate control over the material synthesis (and thus material performance) for a model SEI on a silicon anode. We studied how sputter conditions effect the structure and the composition of lithium silicate thin films through various composition, surface and structure analysis techniques such as ICP-OES, FTIR, TOF-SIMS and XPS. We manufactured five different compositions of lithium silicates films with Li/Si ratios ranging from ~1.5-7.5. We identified the sputter rate for each composition and controlled deposition time to create films with desired thickness. Through our structural analysis in the bulk of the lithium silicate films, we were able to distinguish changes in NBO content across composition and draw conclusions as to how additional lithium content effects the structure of lithium silicates. We observed carbon contamination through the thickness of the film independent of composition, which may indicate the presence of impurities within the targets. However, the changing of the NBO/BO ratio gave confidence that the film structure was changing along the lines expected for increasing lithium content in lithium silicates. This range of compositions of lithium silicates and the detailed understanding of their structures will lend itself to future studies on lithium silicates formed at the interface of silicon anodes and electrolyte in Li-ion batteries.

REFERENCES:

1. Tarascon, J.M. and M. Armand, *Issues and challenges facing rechargeable lithium batteries.* Nature, 2001. **414**(6861): p. 359-367.
2. Etacheri, V., et al., *Challenges in the development of advanced Li-ion batteries: a review.* Energy & Environmental Science, 2011. **4**(9): p. 3243-3262.
3. Park, C.M., et al., *Li-alloy based anode materials for Li secondary batteries.* Chemical Society Reviews, 2010. **39**(8): p. 3115-3141.
4. McDowell, M.T., et al., *25th Anniversary Article: Understanding the Lithiation of Silicon and Other Alloying Anodes for Lithium-Ion Batteries.* Advanced Materials, 2013. **25**(36): p. 4966-4984.
5. Scrosati, B., J. Hassoun, and Y.K. Sun, *Lithium-ion batteries. A look into the future.* Energy & Environmental Science, 2011. **4**(9): p. 3287-3295.
6. Philippe, B., et al., *Role of the LiPF6 Salt for the Long-Term Stability of Silicon Electrodes in Li-Ion Batteries - A Photoelectron Spectroscopy Study.* Chemistry of Materials, 2013. **25**(3): p. 394-404.

7. Jaumann, T., et al., *SEI-component formation on sub 5 nm sized silicon nanoparticles in Li-ion batteries: the role of electrode preparation, FEC addition and binders.* Physical Chemistry Chemical Physics, 2015. **17**(38): p. 24956-24967.
8. Young, B.T., et al., *Hard X-ray Photoelectron Spectroscopy (HAXPES) Investigation of the Silicon Solid Electrolyte Interphase (SEI) in Lithium-Ion Batteries.* Acs Applied Materials & Interfaces, 2015. **7**(36): p. 20004-20011.
9. Pfeiffer, H., P. Bosch, and S. Bulbulian, *Synthesis of lithium silicates.* Journal of Nuclear Materials, 1998. **257**(3): p. 309-317.
10. Carella, E. and M.T. Hernandez, *High lithium content silicates: A comparative study between four routes of synthesis.* Ceramics International, 2014. **40**(7): p. 9499-9508.
11. Chen, A. and P.F. James, *Amorphous Phase-Separation and Crystallization in a Lithium Silicate Glass Prepared by the Sol-Gel Method.* Journal of Non-Crystalline Solids, 1988. **100**(1-3): p. 353-358.
12. Subha, P.V., et al., *Enhanced CO2 absorption kinetics in lithium silicate platelets synthesized by a sol-gel approach.* Journal of Materials Chemistry A, 2014. **2**(32): p. 12792-12798.
13. Mahmoud, M.M., et al., *Crystallization of Lithium Disilicate Glass Using Microwave Processing.* Journal of the American Ceramic Society, 2012. **95**(2): p. 579-585.
14. Buchner, S. and N.M. Balzaretti, *Pressure and temperature stability range of crystalline lithium metasilicate in a binary Li2O center dot 2SiO(2) glass.* Journal of Physics and Chemistry of Solids, 2013. **74**(8): p. 1179-1183.
15. Li, P., B.A. Ferguson, and L.F. Francis, *Sol-Gel Processing of Lithium Disilicate .1. Crystalline Phase Development of Gel-Derived Powders.* Journal of Materials Science, 1995. **30**(16): p. 4076-4086.
16. Furusawa, S.I., A. Kamiyama, and T. Tsurui, *Fabrication and ionic conductivity of amorphous lithium meta-silicate thin film.* Solid State Ionics, 2008. **179**(15-16): p. 536-542.
17. Li, P. and L.F. Francis, *Sol-gel processing of lithium disilicate .2. Crystallization and microstructure development of coatings.* Journal of Materials Science, 1995. **30**(24): p. 6192-6204.
18. Dudney, N.J., J.B. Bates, and J.D. Robertson, *Radiofrequency Magnetron Sputtering of Pure and Mixed Targets of Li4sio4, Li3po4, and Li2o.* Journal of Vacuum Science & Technology a-Vacuum Surfaces and Films, 1993. **11**(2): p. 377-389.
19. Delpuech, N., et al., *Correlation between irreversible capacity and electrolyte solvents degradation probed by NMR in Si-based negative electrode of Li-ion cell.* Electrochemistry Communications, 2013. **33**: p. 72-75.
20. Xun, S., et al., *The Effects of Native Oxide Surface Layer on the Electrochemical Performance of Si Nanoparticle-Based Electrodes.* Journal of the Electrochemical Society, 2011. **158**(12): p. A1260-A1266.
21. Delpuech, N., et al., *Critical Role of Silicon Nanoparticles Surface on Lithium Cell Electrochemical Performance Analyzed by FTIR, Raman, EELS, XPS, NMR, and BDS Spectroscopies.* Journal of Physical Chemistry C, 2014. **118**(31): p. 17318-17331.

22. Cao, C.T., et al., *In Situ Study of Silicon Electrode Lithiation with X-ray Reflectivity.* Nano Letters, 2016. **16**(12): p. 7394-7401.
23. Fuss, T., et al., *Ex situ XRD, TEM, IR, Raman and NMR spectroscopy of crystallization of lithium disilicate glass at high pressure.* Journal of Non-Crystalline Solids, 2006. **352**(38-39): p. 4101-4111.
24. Shevyakov, A.M., et al., *Study of the Structure and Crystallization of Melts of the System Li2o-Sio2 by High-Temperature Infrared Spectroscopy.* Journal of Applied Chemistry of the Ussr, 1978. **51**(11): p. 2493-2496.
25. Yu, B.C., et al., *Effect of oxide layer thickness to nano-Si anode for Li-ion batteries.* Rsc Advances, 2013. **3**(24): p. 9408-9413.
26. Schroder, K.W., et al., *Role of Surface Oxides in the Formation of Solid-Electrolyte Interphases at Silicon Electrodes for Lithium-Ion Batteries.* Acs Applied Materials & Interfaces, 2014. **6**(23): p. 21510-21524.
27. Veith, G.M., et al., *Direct Determination of Solid-Electrolyte Interphase Thickness and Composition as a Function of State of Charge on a Silicon Anode.* Journal of Physical Chemistry C, 2015. **119**(35): p. 20339-20349.
28. Kim, S.Y. and Y. Qi, *Property Evolution of Al2O3 Coated and Uncoated Si Electrodes: A First Principles Investigation.* Journal of the Electrochemical Society, 2014. **161**(11): p. F3137-F3143.
29. Rao, R.P., T.D. Tho, and S. Adams, *Ion transport pathways in molecular dynamics simulated lithium silicate glasses.* Solid State Ionics, 2010. **181**(1-2): p. 1-6.
30. Voigt, U., et al., *Cation clustering in lithium silicate glasses: Quantitative description by solid-state NMR and molecular dynamics simulations.* Physical Review B, 2005. **72**(6).
31. Iwamoto, N., et al., *Molecular-Dynamics Simulation of Li4sio4 Melt and Glass.* Journal of Non-Crystalline Solids, 1987. **95-6**: p. 233-240.
32. Brooker, M.H. and J.B. Bates, *Raman and Infrared Spectral Studies of Anhydrous Li2co3 and Na2co3.* Journal of Chemical Physics, 1971. **54**(11): p. 4788-&.
33. Parker, S.F., et al., *Assignment of the vibrational spectra of lithium hydroxide monohydrate, LiOH center dot H2O.* Journal of Chemical Physics, 2011. **134**(8).
34. Wang, S.N., et al., *Ternary Phase-Separation Investigation of Sol-Gel Derived Silica from Ethyl Silicate 40.* Scientific Reports, 2015. **5**.
35. Li, X.Y. and H.M. Yang, *Morphology-controllable Li2SiO3 nanostructures.* Crystengcomm, 2014. **16**(21): p. 4501-4507.
36. Koroleva, O.N., M.V. Shtenberg, and P.V. Khvorov, *Vibrational spectroscopic and X-ray diffraction study of crystalline phases in the Li2O-SiO2 system.* Russian Journal of Inorganic Chemistry, 2014. **59**(3): p. 255-258.
37. Nocun, M. and M. Handke, *Identification of Li-O absorption bands based on lithium isotope substitutions.* Journal of Molecular Structure, 2001. **596**: p. 145-149.
38. Kelly, M.A., *Analyzing Insulators with XPS and AES*, in *Surface Analysis by Auger and X-ray Photoelectron Spectroscopy*, J.T.G. D. Brigss, Editor. 2003, IM Publications: Chichester. p. 191-210.
39. Metson, J.B., et al., *Suppression of Molecular-Ions in the Secondary Ion Mass-Spectra of Minerals.* Surface and Interface Analysis, 1983. **5**(5): p. 181-185.

40. Meini, S., et al., *Rechargeability of Li-air cathodes pre-filled with discharge products using an ether-based electrolyte solution: implications for cycle-life of Li-air cells.* Physical Chemistry Chemical Physics, 2013. **15**(27): p. 11478-11493.

Built on LDRD Laboratory Directed Research and Development

Sandia National Laboratories is a multimission laboratory managed and operated by National Technology and Engineering Solutions of Sandia LLC, a wholly owned subsidiary of Honeywell International Inc. for the U.S. Department of Energy's National Nuclear Security Administration under contract DE-NA0003525.

Sandia National Laboratories

U.S. DEPARTMENT OF ENERGY